Frequency-dependent electron spin resonance study of P_b-type interface defects in thermal Si/SiO_2

D. Pierreux and A. Stesmans
Department of Physics, University of Leuven, 3001 Leuven, Belgium
(Received 2 May 2002; published 30 October 2002)

A frequency-dependent electron spin resonance (ESR) study has been carried out of inherent Si dangling-bond-type point defects in thermal Si/SiO_2 [P_b in $(111)Si/SiO_2$, P_{b0} and P_{b1} in $(100)Si/SiO_2$], admittedly generated as a result of mismatch induced interface strain. This has enabled the separation of the strain broadening component from other line broadening mechanisms, leading to a direct quantification of the associated interface stress. It is found that the technologically favored $(100)Si/SiO_2$ interface exhibits generally more strain than typical for $(111)Si/SiO_2$. However, the interface strain may be strongly reduced in both structures by appropriate postoxidation anneals. Additionally, information is gained on the spatial distribution of the defects: Strong evidence is provided that P_{b0} and P_{b1} in $(100)Si/SiO_2$ are distributed in a different way than $P_b s$ at the $(111)Si/SiO_2$ interface. Moreover, these distributions are found to be dependent on the thermal history of the sample, i.e., roughness of the interface layer.

DOI: 10.1103/PhysRevB.66.165320 PACS number(s): 68.35.Dv, 73.40.Qv, 76.30.Mi, 61.72.Hh

I. INTRODUCTION

Thermal oxidation of Si is accompanied by the inherent generation of dangling-bond-type defects at the planar Si/SiO_2 interface as a result of lattice-network mismatch between the *c*-Si and *a*-SiO_2.[1] Some types of these coordination point defects are paramagnetic and may thus be detected by electron spin resonance (ESR). At the $(111)Si/SiO_2$ interface only one type of such defect has so far been traced by ESR, specifically referred to as the P_b center.[2,3] Mainly on the basis of ESR measurements the defect has conclusively been identified as an $sp^3_{[111]}$ dangling hybrid on an interfacial Si atom, backbonded to three Si atoms in the bulk, denoted as $^{\bullet}Si{\equiv}Si_3$, where the dot symbolizes the unpaired dangling bond electron.[2–4] It exhibits C_{3v} symmetry and is ESR active when neutral. For as-grown thermal (800–970 °C) oxides a natural density of $N_0 \sim 4.9\times10^{12}\ cm^{-2}$ is inherently incorporated.[5]

The technological dominant $(100)Si/SiO_2$ structure, by contrast, exhibits two prominent ESR-active defects, called P_{b0} and P_{b1}.[6] For standard oxidation temperatures (800–970 °C) a density of $\sim1\times10^{12}\ cm^{-2}$ is found for both defects.[7] As compared to P_b, the way to atomic identification here was much longer, for reasons including the inherently lower defect density and spectral interference. As to P_{b0}, where the ^{29}Si hyperfine structure has first been resolved, the evidence is that it just concerns the equivalent of the P_b defect, but now residing at $(111)Si/SiO_2$-like microfacets at the macroscopic $(100)Si/SiO_2$ interface.[8–10] Regarding P_{b1}, the breakthrough in identification came from the discovery of sample fabrication parameters, i.e., post oxidation anneal in vacuum, that lead predominantly to P_{b1} production, which enabled new systematic observations of the $(100)Si/SiO_2$ interface, including crucial ^{29}Si *hf* structure.[10,11] The P_{b1} defect was identified, like P_b, as a prototype Si dangling-bond defect approximately pointing along a $\langle211\rangle$ direction at ~32° with the [100] interface normal.[12]

Admittedly, interface defects are formed to alleviate interface strain (mismatch), which, at the $(111)Si/SiO_2$ interface, was formerly quantified in terms of the P_b *g*-factor distribution inferred from field angle dependence of the ESR linewidth.[13,14] The latter method was also applied on $(100)Si/SiO_2$ structures which, by appropriate treatments, could be processed to exhibit predominantly either P_{b0} or P_{b1}.[10] However, for standard $(100)Si/SiO_2$, where both defects appear approximately in equal densities, that method becomes unsuitable due to spectral overlap.

In the present study this has been overcome by applying a frequency-dependent ESR study for fixed suitable orientations of the magnetic field, with respect to the Si substrate enabling accurate quantification of strain broadening and ESR line shape, in relationship with sample processing and occurring P_b-type defect densities. This resulted in the observation of some marked differences in the interface nature of the oxidized crystallographic (111) and (100)Si surfaces. Moreover, in both Si/SiO_2 structures a marked influence on the strain broadening component by postoxidation thermal treatment is revealed, indicative of interface relaxation. Additionally, we also observed a correlation between interface strain, interface roughness, and defect distribution, which will be discussed in more detail.

II. EXPERIMENT

A. Sample preparation

The starting substrates were Si slices of $2\times9\text{-}mm^2$ main face cut from commercial two-side polished Czochralski-grown (111) Si (*p* type; >100 Ω cm) and (001) Si wafers (*p* type; ~10 Ω cm). After wet chemical cleaning, the slices were thermally oxidized at $T_{ox}=970$ °C (1.1 atm O_2; 99.9995%) for ~1 h. For $(111)Si/SiO_2$, a first sample (labeled Ia), not submitted to any postoxidation thermal treatment, served as a reference, while for $(100)Si/SiO_2$ a first ESR sample was submitted to hydrogenation (1 atm H_2; 99.9999%) at 795 °C for ~1 h. As after such step, the P_b-type defects are left passivated by H, this was finally followed by a vacuum anneal at 610 °C for ~1 h—a treat-

ment known to exhaustively depassivate (ESR activate) H-passivated P_b-type defects. The hydrogenation/dissociation procedure at the (100) interface was carried out to make an ESR study feasible through enhancement of the defect densities[10] by about a factor 5: For a typical ESR sample, natural P_{b0}, P_{b1} densities in as-grown standard $(100)Si/SiO_2$ appeared too small to enable reliable *Q*-band observations. Although the sample received additional postoxidation (PO) heat treatment, it will be referred to as the (100) reference sample (type Ib).

A second set of samples (type II) was, after oxidation, submitted to a postoxidation vacuum anneal (POVA) at high temperature, i.e., 1200 °C, ~35 min for (111) (sample IIa) and 1130 °C, ~1 h for $(100)Si/SiO_2$ (sample IIb). For $(100)Si/SiO_2$ this was done to maximize the P_{b1} production ($[P_{b1}]/[P_{b0}]>6$). A third (100) sample, labeled III, was oxidized at 180 °C for ~190 min without additional treatment in order to maximize the P_{b0} density ($[P_{b0}]/[P_{b1}]>20$).

B. ESR spectrometry

Conventional absorption-derivative ESR observations were made at ~4.3 < (*X* and *K* band) and ~30 K (*Q*-band). The P_b densities were determined by comparison of the signal intensity I, obtained by double numerical integration of the detected first derivative spectra dP_μ/dB (where P_μ is applied microwave power and **B** the applied magnetic field), to that of a comounted calibrated Si:P standard sample. This was done in the most sensitive setup, the *K*-band spectrometer. For the reference samples (I), defect densities of $\sim 5\times10^{12}$ cm^{-2}, $\sim 5\times10^{12}$ cm^{-2}, and $\sim 7\times10^{12}$ cm^{-2} for P_b, P_{b1}, and P_{b0} were obtained, respectively. The POVA treated samples (II) exhibit a defect density of $\sim 2\times10^{13}$ cm^{-2} and $\sim 4\times10^{12}$ cm^{-2} for P_b and P_{b1}, respectively, while a P_{b0} density of $\sim 6.5\times10^{12}$ cm^{-2} was found in the low-T_{ox} sample (III). As a result of the high saturability of the (100) POVA sample (1130 °C) the determined value for the P_{b1} defect density could still be somewhat underestimated. The absolute accuracy on defect density determination is estimated at ±20%.

In standard $(100)Si/SiO_2$, spectral interference hinders direct determination of the properties of the P_{b0} and P_{b1} ESR signals. Two methods for deconvolution were tried out. In a first approach the sum of two theoretical line shapes, representing P_{b0} and P_{b1}, are fitted to the experimental spectra. Gauss, Lorentz, and Voigt shapes could be chosen in the fit procedure. Although spectra could always be calculated to fit the experimental signals excellently—no wonder in view of the numerous adjustable fitting parameters—this working method had to be discarded as it led to inconsistent data. It sharply exposes the plain unreliability of such fitting procedures—though widely applied—if unaware of the correct line shapes involved. Insight came from additional measurements made on sample III with the large incorporated P_{b0} density. These spectra revealed the highly *asymmetric* character of the P_{b0} resonance line, incompatible with any of the standard theoretical shapes, which are all symmetric. Hence this invalidates such fitting procedure based on fitting symmetric curves.

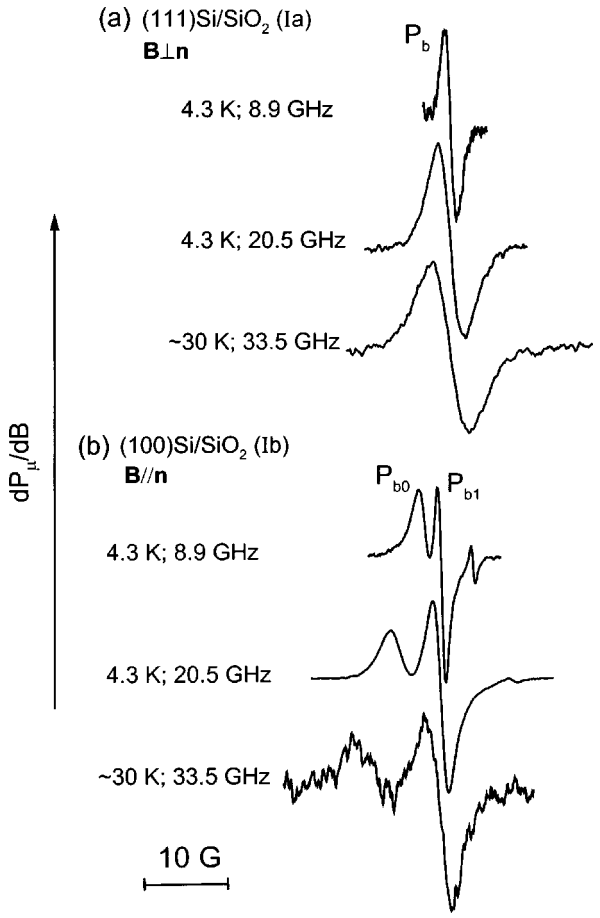

FIG. 1. Observed ESR spectra of P_b-type defects in the reference samples (Ia, Ib), showing the influence of observational frequency ν: (a) P_b with $\mathbf{B}\|(111)Si/SiO_2$ interface (sample Ia), (b) P_{b0} and P_{b1} with $\mathbf{B}\perp(100)Si/SiO_2$ (Ib).

In a second working approach the starting point, hinted by the experiment, is the assumption of a highly symmetric P_{b1} signal. After fitting, this is substracted from the experimental spectrum to resolve the P_{b0} signal. The used criteria here for a reliable simulation were the smoothness of the remaining P_{b0} signal together with its characteristic asymmetric feature. The fitting was performed by slightly varying the parameters (linewidth, shape, intensity, *g* value) of the P_{b1} resonance until an optimum P_{b0} line appeared. This fitting procedure resulted in inference of consistent data over the various recorded spectra.

III. EXPERIMENTAL RESULTS

A. Reference samples

Figure 1 illustrates the influence of the resonance frequency ν on the ESR signals of P_b for $\mathbf{B}\perp\mathbf{n}$ (within ~3°)the interface normal, and those of P_{b0} and P_{b1} for $\mathbf{B}\|\mathbf{n}$ in $(111)Si/SiO_2$ (Ia) and $(100)Si/SiO_2$ (Ib) samples, respectively. The spectra reveal large differences in line shape and linewidth, which will both be analyzed below.

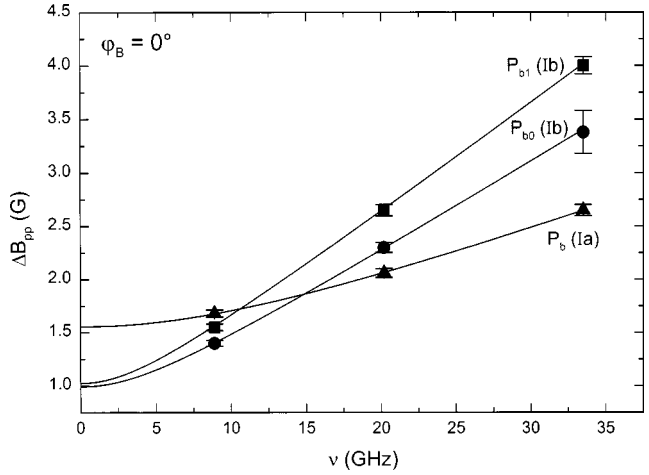

FIG. 2. Frequency dependence of the P_b-type ESR peak-to-peak linewidth in the reference samples (Ia and Ib) for $\varphi_B=0°$. Solid lines represent least-squares fits using Eq. (4).

The behavior of the measured first derivative peak-to-peak linewidth $\Delta B_{\rm pp}$ as a function of ν (observational frequency) for **B** parallel to the sp^3 dangling-bond directions ($\varphi_B=0°$) is shown in Fig. 2: φ_B represents the angle between the defect dangling-bond direction and **B**. We note two clear trends: First, there is the expected general increase in the linewidths with frequency resulting from the existence of a strain induced, admittedly, Gaussian spread in $g_\perp$ and $g_\parallel$ (see next section). Second, changing the crystallographic orientation has a clear impact: While the overall linewidth of both P_{b0} and P_{b1} is broader at high frequencies, it drops below the P_b value for $\nu\sim 8.9$ GHz ($\nu\rightarrow 0$) hinting at a smaller residual linewidth, i.e., width without strain broadening.

Figure 3 shows the behavior of $\Delta B_{\rm pp}$ of P_{b0} and P_{b1} in reference sample Ib as a function of frequency for

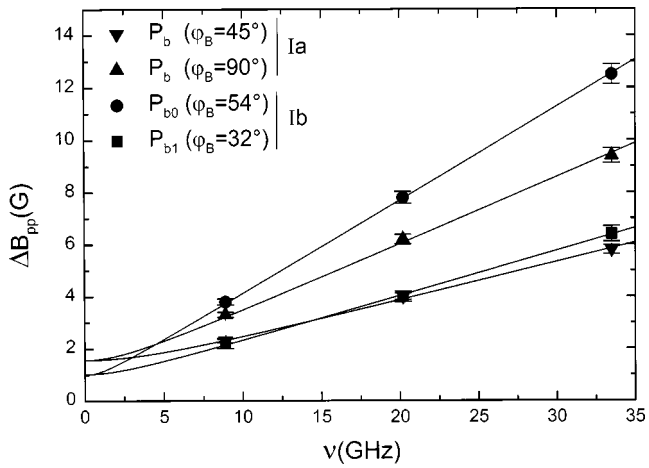

FIG. 3. Frequency dependence of the P_{b0}, P_{b1} ESR peak-to-peak linewidth in the reference sample (Ib) for $\mathbf{B}\perp(100)\mathrm{Si/SiO_2}$ corresponding with $\varphi_B\sim 54°$ and $\varphi_B\sim 32°$ for P_{b0} and P_{b1}, respectively. The data obtained for P_b in the $(111)\mathrm{Si/SiO_2}$ reference sample (Ia) for $\varphi_B=45°$ and $\varphi_B=90°$ are also plotted. Solid lines represent least-squares fits using Eq. (4).

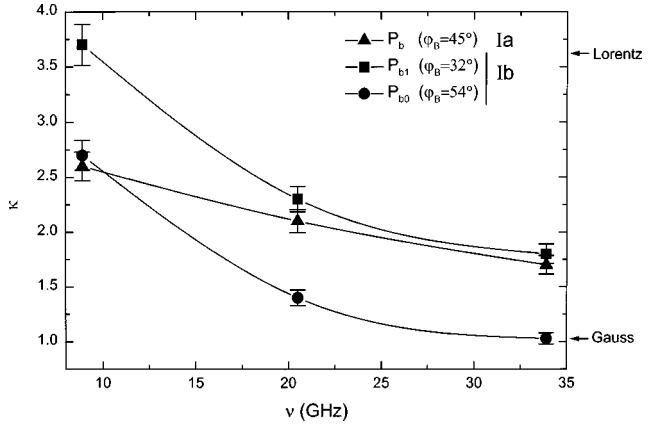

FIG. 4. Frequency dependence of the P_{b0}, P_{b1} ESR line-shape factor κ for $\mathbf{B}\|\mathbf{n}$ in the $(100)\mathrm{Si/SiO_2}$ reference sample (Ib), and of P_b in reference sample (Ia) for $\varphi_B=45°$.

$\mathbf{B}\perp(100)\mathrm{Si/SiO_2}$ interface ($\mathbf{B}\|\mathbf{n}$), corresponding to $\varphi_B\sim 32°$ and $\sim 54°$ for P_{b1} and P_{b0}, respectively. This is the orientation where the different branches in the g maps for each of the P_{b0} and P_{b1} defect coincide (cf. Fig. 1), enabling the most accurate determination of the linewidths. Also added are the P_b $\Delta B_{\rm pp}$ values observed in the reference sample $(111)\mathrm{Si/SiO_2}$ (Ia) for $\varphi_B=45°$ and 90°. Clearly, the leading trend is a marked increase in linewidth with increasing frequency. Interestingly, we additionally notice distinct variations dependent on crystallographic orientation and defect type. In particular, as to the $(100)\mathrm{Si/SiO_2}$ defects, the increase is stronger for P_{b0} than P_{b1}, while, in turn, the ν dependence is generally more prominent for the (100) face as compared to (111).

In Fig. 4 is illustrated, for the reference samples, for some specific φ_B values the effect of observational frequency on the line-shape factor κ, defined as $\kappa=1/A_{\rm pp}(\Delta B_{\rm pp})^2$, where $A_{\rm pp}$ is the peak-to-peak signal height and I the signal intensity (area under the absorption curve). The measured κ values are seen to span the range from the Gaussian line-shape factor ($\kappa^G=1.03$), observed at the highest frequency for P_{b0}, to the Lorentzian value ($\kappa^L=3.63$) pertaining to the lowest frequency for P_{b1}. Three trends are clearly observed: First, for the defects at both interface orientations there is a general decrease in κ with increasing frequency caused by the rising admixture of the Gaussian strain broadening component (see next section), competing with the residual Lorentzian part, with an attendant change in shape of the resonance signal. Second, for a fixed frequency, P_{b0} generally exhibits a lower κ value than P_{b1}. Three, the P_b signal at the (111) interface shows a distinctly less pronounced drop in κ with increasing frequency as compared to P_{b0}, P_{b1}.

B. Other samples

Figure 5 shows some typical ESR line shapes of P_b-type defects observed in the POVA samples (II) and the low-$T_{\rm ox}$ sample (III). The effect of POVA on the P_b ESR linewidth (sample IIa) for $\varphi_B=0°$ and 90° is illustrated in Fig. 6. As compared to the P_b reference data (Ia) we notice a marked drop in the *slope* of the $\Delta B_{\rm pp}$-vs-ν data for $\varphi_B=90°$—much

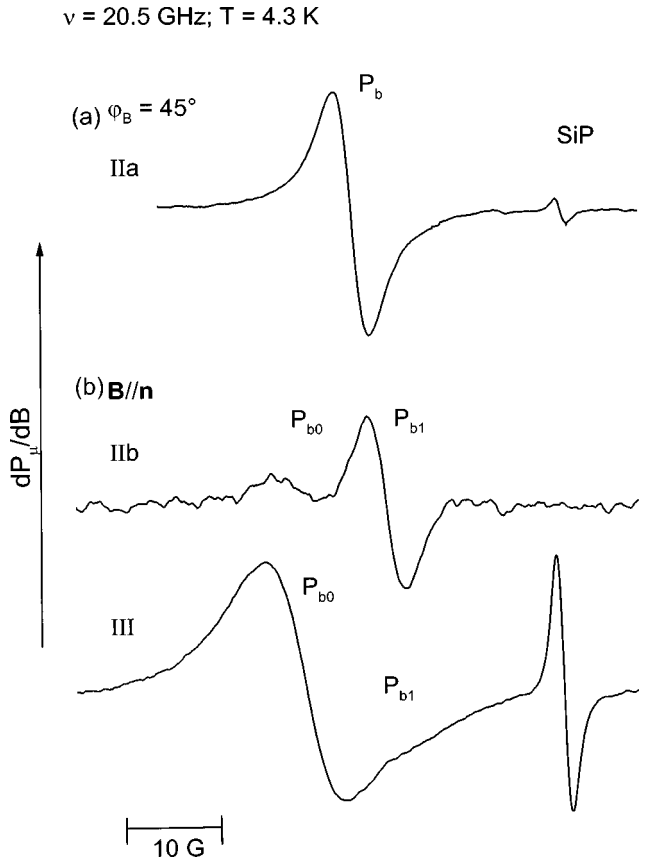

FIG. 5. *K*-band ESR spectra of nonreference samples: (a) P_b in $(111)\mathrm{Si/SiO_2}$ sample IIa, i.e., sample Ia additionally submitted to POVA at 1200 °C, (b) P_{b1} and P_{b0} in sample IIb, i.e., sample Ib submitted to POVA at 1130 °C, and P_{b0} in the low-T_{ox} sample (III). The Si:P signal stems from a comounted marker sample.

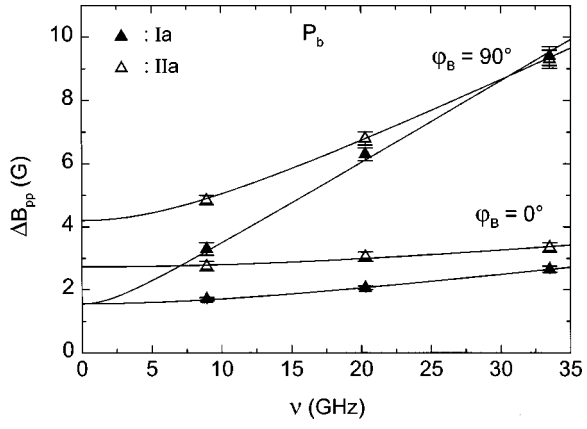

FIG. 6. Frequency dependence of the ESR peak-to-peak linewidth of P_b observed in the $(111)\mathrm{Si/SiO_2}$ POVA sample (IIa). Solid lines represent least-squares fits using Eq. (4). For comparison, the data of the $(111)\mathrm{Si/SiO_2}$ reference sample (Ia) are also included (cf. Figs. 2 and 3).

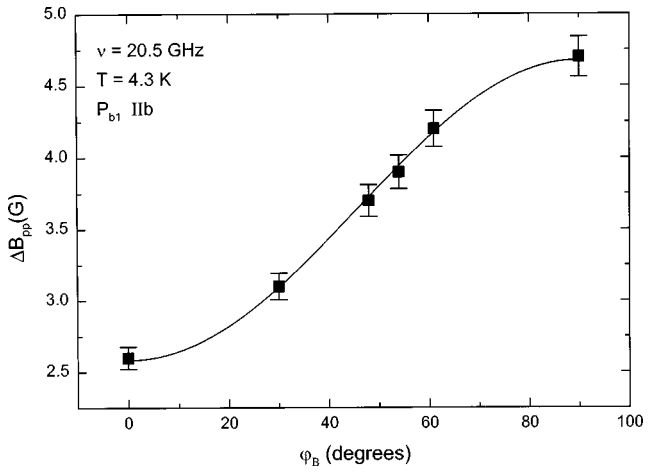

FIG. 7. Magnet angle dependence of the ESR linewidth of P_{b1} in $(100)\mathrm{Si/SiO_2}$ subjected to POVA at 1130 °C (sample IIb). The angle φ_B is referred to the dangling-bond defect direction (**B**∥[211] within 3°). The solid line represents a least-square fit of the data using Eq. (4).

less though for $\varphi_B = 0°$. Additionally, a general increase in residual linewidth $[\Delta B_{\mathrm{pp}}(\nu = 0)]$ appears as a result of POVA for both magnetic-field directions.

The frequency dependence of the P_{b1} linewidth was studied in detail in the (100) POVA sample (IIb). However, due to the high saturability, the P_{b1} signal width could only be accurately measured at *K* band, resulting in the angular map of the linewidth shown in Fig. 7. From these data, the frequency-dependent behavior of ΔB_{pp} for P_{b1} was determined using the fitting procedure outlined in the next section. This result is shown in Fig. 8 (dashed curve) for the case **B**∥**n**, together with the (100) reference sample data (Ib). Interestingly, we notice for the (100) POVA sample the same

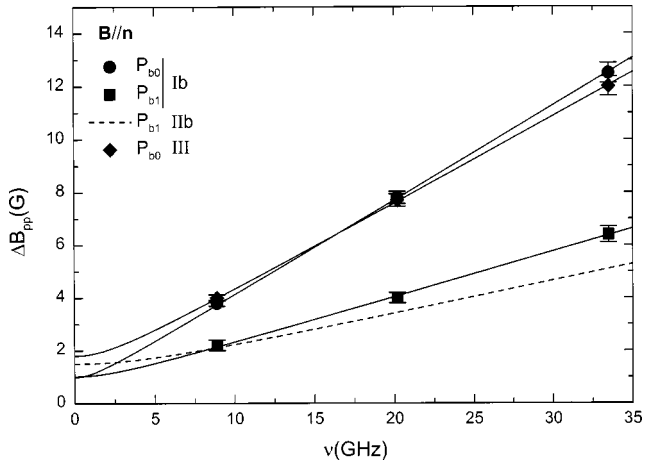

FIG. 8. Frequency dependence of the ESR peak-to-peak linewidth of P_{b1} and P_{b0} observed in the (100) POVA sample (IIb) and low-T_{ox} sample (III) for **B**⊥$(100)\mathrm{Si/SiO_2}$ interface, respectively. Solid lines represent least-squares fits using Eq. (4). The dashed curve, corresponding to P_{b1}, is obtained from Eq. (4) using the parameters inferred from fitting the angular dependence (cf. Fig. 7). For comparison, the data of the $(100)\mathrm{Si/SiO_2}$ reference sample (Ib) are also included (cf. Fig. 2).

effects as for the (111)Si/SiO_2 POVA sample (cf. Fig. 6), i.e., as to P_b, decrease in the slope of the ΔB_{pp}-vs-ν data and increased residual linewidth [$\Delta B_{pp}(\nu=0)$].

The frequency dependence of ΔB_{pp} [$\mathbf{B}\perp$(100)Si/SiO_2 interface] for P_{b0} in the low-T_{ox} sample (III) is also plotted in Fig. 8. Though the change of the slope, as compared to the reference sample data, is rather low, there again appears a significant increase in the extrapolated ($\nu\rightarrow 0$) ΔB_{pp} value as a result of the POVA treatment.

IV. ANALYSIS AND DISCUSSION

A. Fitting procedure

From field-angle-dependent observations, a previous study had concluded that the P_b ESR linewidth at the standard (111)Si/SiO_2 interface consists of mainly two superimposed contributions:[13,14] In addition to an angle-independent residual part, there is a considerable Gaussian-type broadening monotonically growing for **B** tilting away from **n**. The Gaussian part is attributed to strain induced variations in the g matrix, predominantly in $g_\perp$, based on the insight provided by molecular orbital calculations[15] that variations in the microscopic geometry of a dangling-bond-type defect results in a perturbation in $g_\perp$, but not, to first order, in $g_\parallel$, leading to a distribution in the resonance g value. The supposedly Lorentzian residual linewidth ($\nu\rightarrow 0$) contribution was mainly attributed to unresolved ^{29}Si superhyperfine broadening. A later, more in-depth line-shape study of the residual line for $\mathbf{B}\perp$(111)Si/SiO_2 interface revealed clearly the influence of a relative small P_b-density-dependent dipolar broadening.[16] Importantly, in Ref. 5 also the presence of some strain-induced spread in $g_\parallel$ was demonstrated on the as-oxidized P_b ESR line shape. As it appeared that the kernel of all three defects P_b, P_{b0}, P_{b1} is chemically identical, i.e., dangling bonds with generic entity $\equiv$Si$^{\cdot}$, it is reasonable to assume that the linewidths of P_{b0} and P_{b1} can be approached in the same manner as P_b.

As mentioned in the introduction it is our aim to quantify the interface strain, in terms of their g-factor distribution, based on frequency measurements instead of the formerly used field-angle dependence of the linewidth. In fitting the data, two approximations are made: First, it is assumed that the frequency-independent part, consisting of mainly ^{29}Si superhyperfine and dipolar broadening, is purely Lorentzian and void of strain effects; second, the strain component ΔB_{pp}^{SB} is Gaussian and can be related to a Gaussian distribution in $g_\parallel$ and $g_\perp$. To a first approximation, the frequency dependence of ΔB_{pp}^{SB} can be expressed as

$$\Delta B_{pp}^{SB}=\frac{2h\nu}{\beta}\left(\frac{g_\parallel\cos^2\varphi_B}{g^3}\sigma g_\parallel+\frac{g_\perp\sin^2\varphi_B}{g^3}\sigma g_\perp\right), \quad (1)$$

where $\sigma g_\parallel$ and $\sigma g_\perp$ are the standard deviations of the Gaussian distributions in $g_\parallel$ and $g_\perp$, respectively. This is a generalized approach of the one presented in Ref. 13 were $\sigma g_\parallel=0$ was assumed. The g map of a dangling-bond defect, with axial symmetry, for rotation of **B** from $\mathbf{B}\parallel$dangling bond ($\varphi_B=0°$) towards $\mathbf{B}\perp$dangling bond ($\varphi_B=90°$) obeys

$$g=\sqrt{(g_\parallel\cos\varphi_B)^2+(g_\perp\sin\varphi_B)^2}. \quad (2)$$

For g values we insert $g_\parallel=2.001\,36$, $g_\perp=2.0088$ for P_b,[5] $g_\parallel=2.0022$, $g_\perp=2.0058$ (rounded to axial symmetry) for P_{b1}, and $g_\parallel=2.001\,85$, $g_\perp=2.0081$ for P_{b0}.[10] The measured convolution of the frequency-independent Lorentzian part and the Gaussian strain component is expected to be largely Voigt-like. Using then the accurate formula

$$\Delta B_{pp}=\frac{1}{2}\Delta B_{pp}^L+\left((\Delta B_{pp}^G)^2+\frac{1}{4}(\Delta B_{pp}^L)^2\right)^{1/2}, \quad (3)$$

where ΔB_{pp}, ΔB_{pp}^L, and ΔB_{pp}^G represent the total, Lorentzian, and Gaussian linewidths of the Voigt shape, allows us, after inserting Eq. (2) for g in Eq. (1) and substituting Eq. (1) for ΔB_{pp}^G in Eq. (3), to obtain our fit function,

$$\Delta B_{pp}=\frac{1}{2}\Delta B_{pp}^L+\left\{\left[\frac{2h\nu}{\beta}\left(\frac{g_\parallel\cos^2\varphi_B}{g^3}\sigma g_\parallel+\frac{g_\perp\sin^2\varphi_B}{g^3}\sigma g_\perp\right)\right]^2+\frac{1}{4}(\Delta B_{pp}^L)^2\right\}^{1/2}. \quad (4)$$

The ΔB_{pp}-vs-ν data of Figs. 2, 3, 6, and 8 and the ΔB_{pp}-vs-φ_B data of Fig. 7 were least-squares fitted with this formula (results shown as solid curves in the figures) from where, generally, the parameters ΔB_{pp}^L, $\sigma g_\parallel$, and $\sigma g_\perp$ are inferred.

B. Reference samples

For $\varphi_B=0°$ (Fig. 2) the fitting resulted in the optimized values $\Delta B_{pp}^L=1.0\pm0.1$ G, $\sigma g_\parallel=0.000\,24\pm0.000\,02$ for P_{b0}, and $\Delta B_{pp}^L=1.05\pm0.1$ G, $\sigma g_\parallel=0.000\,29\pm0.000\,02$ for P_{b1}, that is, very similar values for both defects. These values may be compared to $\Delta B_{pp}^L=1.55\pm0.1$ G, $\sigma g_\parallel=0.000\,14\pm0.000\,01$ found for P_b at the reference (111)Si/SiO_2 interface for $\varphi_B=0°$ (Fig. 2). Although the spread in $g_\parallel$ is considered a second-order effect, $\sigma g_\parallel$ appears distinctly larger at the (100) interface, for both P_{b0} and P_{b1}.

The obtained ΔB_{pp}^L values can be read at the intercept of the fitted curves [Eq. (4)] with the ΔB_{pp} axis (cf. Fig. 2) in the ΔB_{pp}-vs-ν plots as a direct result of the assumption that the Lorentzian part is frequency independent. Indeed, the fit equation (4) shows that extrapolation towards $\nu=0$ leads to $\Delta B_{pp}=\Delta B_{pp}^L$. This remaining component, void of strain influence, represents the residual linewidth composed, as aforementioned, of mainly unresolved ^{29}Si superhyperfine ΔB_{pp}^{int} (intrinsic part) and dipolar broadening ΔB_{pp}^{dip} (dipolar part). In a first approximation, the Lorentzian addition rule is used to separate the latter two parts,

$$\Delta B_{pp}^L=\Delta B_{pp}^{int}+\Delta B_{pp}^{dip}. \quad (5)$$

Comparing the two interface orientations we thus find a drop ($\sim$0.5 G) in ΔB_{pp}^L of P_{b0}, P_{b1} [(100) interface] as compared to P_b. As the kernel of all three defect structures is identical, i.e., silicon dangling bonds, we favor the interpretation that the difference is of dipolar origin rather than intrinsic.

The size of ΔB_{pp}^{dip} for P_b was inferred in a previous study[16] as a function of areal P_b-defect density. For an as-

oxidized sample of $[P_b]\sim 5\times 10^{12}\ \mathrm{cm}^{-2}$ a dipolar line broadening of ~0.4 G may be expected for the case $\varphi_B = 0°$. Inserting this value in Eq. (5) leads to an intrinsic linewidth ΔB_{pp}^{int} (void of strain and dipolar broadening) of ~1.15 G for P_b. If assuming a more or less equal intrinsic linewidth for all three defects, this result suggests a negligible dipolar contribution in the linewidth of P_{b0} and P_{b1} at the $(100)Si/SiO_2$ interface, which result may appear surprising as the density of each of the P_{b0} and P_{b1} defect is also $\sim 5\times 10^{12}\ \mathrm{cm}^{-2}$. As to our knowledge, no separate study of dipolar interactions of P_{b0}, P_{b1} defects in $(100)Si/SiO_2$ has yet been carried out, there exists no independent verification. This merits further perusal.

For practical calculations, the local magnetic field B_{dip} sensed by a dipole μ_k due to the vicinity of surrounding dipoles μ_j is approximated by the sum of their independent static contributions B_{jk}, parallel to the applied field **B**, i.e., $B_{dip}=\Sigma_j B_{jk}$. From the classical expression for the magnetic dipole-dipole (DD) interaction energy one can show that

$$B_{jk}=\pm\frac{3}{2}\frac{g\beta}{2\pi r_{jk}^3}(1-3\cos^2\theta_{jk}), \tag{6}$$

where θ_{jk} is the angle between **B** and the vector $\mathbf{r_{jk}}$ interconnecting the two magnetic moments.

There are essentially three features to which changes in dipolar contribution may be linked. An obvious first one is defect density. In the case of an homogeneous areal defect distribution this possibility has to be excluded because of the determined defect densities: The latter are more or less the same for all three types of P_b defects and thus cannot cause such changes in residual linewidth.

A second possibility is that the defect centers are inhomogeneously distributed over the two-dimensional (2D) interfacial layer. To explain then the differences between (100) and $(111)Si/SiO_2$ interfaces one might presume P_b defects to show a tendency to clustering, i.e., enhanced local defect density and *a fortiori*, larger dipolar contribution, while the $(100)Si/SiO_2$ interface defects would be more homogeneously spread. This, however, is also unlikely, as a previous study provided evidence that the P_b defects in $(111)Si/SiO_2$ are distributed rather evenly in a self-avoiding manner.[16,17]

Third, the observed difference could concern a dimensional aspect. A former study provided strong evidence that (111) P_b defects reside at atomically flat interfacial terraces, in a true two-dimensional (2D) arrangement.[18] If the $(100)Si/SiO_2$ interface would exhibit some (enhanced) 3D aspect the defect distribution could extend over several atomic planes rather than one, ideally. Obviously, for a fixed number of spins, this would result in a distinct reduction of the DD broadening through the $1/r^3$ dependence of DD interaction [see Eq. (6)]. As evidenced in the next section, the latter possibility is considered likely.

The $\sigma g_\perp$ value was derived for $\mathbf{B}\perp(100)Si/SiO_2$ and $\mathbf{B}\parallel(111)Si/SiO_2$, with $\sigma g_\parallel$ and ΔB_{pp}^L kept fixed at the values inferred from the fit for the $\varphi_B=0°$ case, and varying only $\sigma g_\perp$. Keeping ΔB_{pp}^L fixed is justified as the dipolar broadening is only weakly anisotropic for the present defect densities.[17] The obtained fitting values are $\sigma g_\perp = 0.0014 \pm 0.0001$ and 0.0010 ± 0.0001 for P_{b0} ($\varphi_B=54°$) and P_{b1} ($\varphi_B=32°$), respectively. In comparison with the obtained $\sigma g_\perp = 0.000\,76\pm 0.000\,02$ for P_b ($\varphi_B=90°$), these values show that, interestingly, $(100)Si/SiO_2$ exhibits generally higher local interface strain induced variations in defect environment as compared to $(111)Si/SiO_2$. The size of the site-dependent modulation appears also defect-type dependent as shown by difference in the $\sigma g_\perp$ values of P_{b0} and P_{b1}.

C. Other samples

Fitting Eq. (4) to the angular data (cf. Fig. 7) of the (100) sample subjected to POVA (IIb, maximum P_{b1} density) gave for P_{b1} $\Delta B_{pp}^L = 1.5\pm 0.1$ G, $\sigma g_\perp = 0.000\,54\pm 0.000\,02$ and $\sigma g_\parallel = 0.000\,29\pm 0.000\,02$, which may be compared with the reference sample (Ib) values 1.05, 0.0010, and 0.000 29, respectively (see Table I); $\sigma g_\parallel$ is thus found unaltered—not unexpected as $g_\parallel$ is inherently less sensitive to strain. However, a remarkable observation is the drastic drop in $\sigma g_\perp$ induced by the POVA treatment, indicative of the occurrence of stress relaxation at the $(100)Si/SiO_2$ interface. This effect is also observed for P_b at the (111) plane after 1200 °C POVA (sample IIa) (cf. Fig. 6): While the inferred $\sigma g_\parallel = 0.000\,14\pm 0.000\,01$ remains more or less constant, there appears a drop of $\sigma g_\perp$ from $0.000\,76\pm 0.000\,02$ to $0.000\,46 \pm 0.000\,02$ after 1200 °C POVA. As a second result, we thus find that although the P_b and P_{b1} $\sigma g_\perp$ values for both reference samples interfaces are much different, high-temperature treatment in vacuum (inert gas) reduces them down to a more or less equal value. This $\sigma g_\perp$ value could correspond to the lowest possible intrinsic stress in both structures.

Finally, we notice that upon POVA the residual line width ΔB_{pp} ($\nu\to 0$) for P_{b1} (IIb) increases, without increase in defect density, from 1.05 ± 0.10 G to 1.5 ± 0.1 G (cf. Fig. 8). Within the dipolar model, the latter result would indicate that POVA for $(100)Si/SiO_2$ leads to a more two-dimensional defect distribution, i.e., *flatter* interface.

As to P_b, analysis of the $(111)Si/SiO_2$ POVA sample (IIa) data also reveals an increase in residual linewidth from ~1.5 G up to ~2.8 G ($\varphi_B=0°$) and ~4.2 G ($\varphi_B=90°$) (cf. Fig. 6). In the present case, this is ascribed to enhanced dipolar interactions due to the strongly increased P_b defect density, i.e., $\sim 2\times 10^{13}\ \mathrm{cm}^{-2}$ vis-à-vis $\sim 5\times 10^{12}\ \mathrm{cm}^{-2}$ in reference sample I. Indeed, the map of the ΔB_{pp}-vs-φ_B data (not shown) now clearly reveals anisotropic dipolar broadening.[17]

For the low-T_{ox} sample (III) we also observe a drastic increase in P_{b0} residual line width ΔB_{pp} ($\nu\to 0$) towards ~1.8 G (cf. Fig. 8; Table I) as compared to the reference sample (~1.05 G), indicating once more that the interface topography is strongly treatment dependent for $(100)Si/SiO_2$ interfaces. For $\sigma g_\perp$, a small decrease is inferred, i.e., from 0.0014 to 0.0012 ± 0.0001, on the edge of experimental accuracy. The obtained values for $\sigma g_\parallel$, $\sigma g_\perp$, and ΔB_{pp}^L of all three P_b-type defects in differently prepared and treated Si/SiO_2 interfaces are summarized in Table I.

TABLE I. Comparison of inferred $\sigma g_{\parallel}$, $\sigma g_{\perp}$, $\Delta B_{\mathrm{pp}}^{L}$ values of P_b-type defects at the (100) and (111)Si/SiO_2 interfaces over different (thermal) sample treatments and data set fittings.

Treatment	Reference	Fit	$\sigma g_{\parallel}$	$\sigma g_{\perp}$	$\Delta B_{\mathrm{pp}}^{L}$ (G)
		(111)Si/SiO_2: P_b			
$T_{\mathrm{ox}}=850\,^{\circ}\mathrm{C}$.	14	ΔB_{pp}-vs-φ_B		~0.000 80	
$T_{\mathrm{ox}}=900\,^{\circ}\mathrm{C}$	13	ΔB_{pp}-vs-φ_B		0.000 75 ±0.000 10	
$T_{\mathrm{ox}}=651\,^{\circ}\mathrm{C}$	5	signal simulation[a]	~0.000 16		
$T_{\mathrm{ox}}=970\,^{\circ}\mathrm{C}$	18	complex fit[b]	0.000 15 ±0.000 02	0.000 74 ±0.000 02	
$T_{\mathrm{ox}}=970\,^{\circ}\mathrm{C}$ (Ia)	this work	ν	0.000 14 ±0.000 01	0.000 76 ±0.000 02	1.55 ±0.10
$T_{\mathrm{ox}}=970\,^{\circ}\mathrm{C}$; POVA 1200 °C (IIa)	this work	ν	0.000 14 ±0.000 01	0.000 46 ±0.000 02	2.8, 4.2 ±0.1
		(100)Si/SiO_2: P_{b0}			
P_{b0}					
$T_{\mathrm{ox}}=170\,^{\circ}\mathrm{C}$	10	φ_B		0.000 90 ±0.000 05	
$T_{\mathrm{ox}}=180\,^{\circ}\mathrm{C}$ (III)	this work	ν	0.000 24 ±0.000 02	0.0012 ±0.00 01	1.80 ±0.15
$T_{\mathrm{ox}}=970\,^{\circ}\mathrm{C}$; H_2 at 795 °C POVA 610 °C (Ib)	this work	ν	0.000 24 ±0.000 02	0.0014 ±0.00 01	1.0 ±0.1
		(100)Si/SiO_2: P_{b1}			
$T_{\mathrm{ox}}=970\,^{\circ}\mathrm{C}$; POVA 1200 °C	10	φ_B[c]		0.000 35 ±0.000 05	
$T_{\mathrm{ox}}=970\,^{\circ}\mathrm{C}$; H_2 at 795 °C POVA 610 °C (Ib)	this work	ν	0.000 29 ±0.000 02	0.0010 ±0.0001	1.05 ±0.1
$T_{\mathrm{ox}}=970\,^{\circ}\mathrm{C}$; POVA 1130 °C (IIb)	this work	φ_B, ν	0.000 29 ±0.000 02	0.000 54 ±0.000 02	1.5 ±0.1

[a]Spectra were simulated by a convolution of an intrinsic Lorentz and a strain-induced semi-Gaussian component characterized by the spread $\sigma g_{\perp}$.

[b]Obtained within the framework of a computational model based on the magnetostatic approximation of the local magnetic field.

[c]In contrast with all previous measurements (conventional unsaturated absorption-derivative ESR spectroscopy), this result was obtained on ESR data measured by high-power (saturation) second-harmonic detection.

V. INTERPRETATION

A. Defect distribution

First, we address the marked difference in inferred residual linewidth ($\nu \to 0$) for P_b at the (111)Si/SiO_2 (1.55 G) and P_{b0}, P_{b1} at the (100)Si/SiO_2 interface (~1.0 G) for the reference samples (I) (cf. Fig. 2; Table I). As alluded in the previous sections the deviations are ascribed to changes in dipolar interaction. However, as the effect of defect density is excluded, it likely originates from variations in the particular defect distributions over both interfaces. In support of the former idea we refer to a study on the effects of postoxidation annealing on Si/SiO_2 interface roughness.[19,20] There an oxidation model was developed existing of two competing effects: An oxidation induced roughening and a diffusion-related smoothening (step motion). The process is described by a Langevin equation

$$\frac{\partial h(x,y)}{\partial t} = \mu \nabla^2 h(x,y) + \eta(x,y,t), \tag{7}$$

where $h(x,y)$ is the interface height, μ is the step diffusion coefficient and $\eta(x,y,t)$ is a noise term describing the oxi-

dation of silicon. The first term on the right-hand side corresponds with the diffusion induced smoothening and the second to the roughening process of silicon oxidation. Solving Eq. (7) resulted in an rms interface roughness σ,

$$\sigma \propto \left(\frac{\lambda^2}{\mu} t \right)^{1/4}, \tag{8}$$

where t is the oxidation time and λ the oxidation rate.

In Ref. 20, transmission electron microscopy (TEM) pictures revealed that as oxidized ($T_{ox}=900\,°C$) (100)Si/SiO_2 interfaces are rougher than (111)Si/SiO_2 ones. This was quantified in terms of σ inferred as $\sim$0.6 nm for (111) Si/SiO_2 and $\sim$1.5 nm for (100)Si/SiO_2. The observation was explained by the difference in free energy of both interfaces. Thermodynamic smoothing can occur already during oxidation at the more stable (111) interface, with lower free energy, whereas postoxidation annealing in inert ambient is necessary to smooth the (100) silicon. The latter observation complies with our outlined model (previous section) that the (100)Si/SiO_2 defect distribution would exhibit an enhanced 3D aspect, leading to a higher mean interdefect distance and, consequently, a smaller dipolar linewidth contribution.

The results for the POVA samples (II) may be interpreted with the same work[20] as reference. In that work, after a POA in nitrogen at 900 °C, a remarkable observation was that the interface roughness of the (100)Si/SiO_2 sample ($T_{ox}=900\,°C$) was drastically reduced from $\sigma\sim1.5$ nm towards $\sigma\sim0.75$ nm. This has been confirmed, for anneal in Ar, in later work using difference x-ray reflectivity technique.[21] In contrast, an identical treatment did not result in a marked effect at the (111)Si/SiO_2 interface, i.e., σ remained fixed at 0.6 nm. The former results are in accordance with the present findings: First, regarding (111)Si/SiO_2, where the interface roughness remains constant after POA, we ascribe the substantially enlarged residual linewidth for P_b to enhanced DD broadening as a result of the drastic increase in defect density up to $\sim 2\times10^{13}$ cm^{-2} (IIa). Second, there is the other fact that after POA of (100)Si/SiO_2 the interface roughness dropped to a value close to that of as oxidized (111)Si/SiO_2 [$\sigma\sim0.6$, ~0.75 for (111), (100)Si/SiO_2, respectively]:[20] This we also find mirrored in the inferred residual linewidths of P_b and P_{b1} in samples Ia and IIb [ΔB_{pp} ($\nu=0$)$\sim$1.55, 1.5 for P_b, P_{b1}, respectively] as the P_b and P_{b1} defect densities are about the same ($\sim 5\times10^{12}$ cm^{-2}). The latter indicates that, like P_b at the (111)Si/SiO_2 interface,[16,17] $P_{b1}s$ also appear organized in a self-avoiding manner.

A final observation is the high residual linewidth for P_{b0} in the low-T_{ox} (100)Si/SiO_2 sample (III) as compared to the reference sample Ib ($T_{ox}=970\,°C$), i.e., 1.80 and 1.0 G, respectively. This result is consistent with the notion that the oxidation process is intrinsically roughening.[22] Indeed, in Eq. (8) σ is proportional to the square root of the oxidation rate: The low-T_{ox} sample had a low oxidation rate, which would thus lead to a smoother (100)Si/SiO_2 interface, and hence enhanced dipolar broadening.

B. Interface strain

Here, we first address the impact of high-temperature anneal in vacuum on both (100) and (111) interfaces (cf. data on P_b and P_{b1}, Table I). Several studies have reported on the observation of an intrinsic SiO_2 film stress resulting from thermal oxidation of Si.[23–26] The origin of this stress has been attributed to the 120% molar volume expansion which results from the conversion of Si to SiO_2. According to the simple Maxwell viscoelastic model of a solid, stress relaxation can occur by ''viscous motion''[27] within a-SiO_2 layers away from the growth interface. If assuming the rate of stress relief to be proportional to the stress (as is usually the case), then

$$\frac{d\sigma_i}{dt} = -\frac{\sigma_i}{\Gamma}, \tag{9}$$

where Γ is a constant, namely the viscoelastic relaxation time, and σ_i is the intrinsic growth stress, i.e., the stress that is generated through the film growth process. Integrating Eq. (9) gives the expression $\sigma_i(t)=\sigma_i(0)\exp(-t/\Gamma)$ for the stress relief process, where $\sigma_i(0)$ is the maximum intrinsic stress at the growth interface and t the oxidation or annealing time.

For the reference samples (I), the outer surface of the growing Si/SiO_2 film has been annealed at T_{ox} for the entire period of oxidation, whereas little so occurred for the oxide layers near the final interface. Consequently, virtually no stress relaxation has occurred near the interface region leading to a highly stressed interface.[28] This is mirrored in $\sigma g_\perp$: the in-plane stress leads to variations in the defect's local environment over the interface, resulting in slight modification of g tensors.

Within this model, the high-temperature POVA results (IIa, 1200 °C and IIb, 1130 °C) become clear: Without further influx of O_2, both interfaces may relief stress for $\sim$1 h. At the high temperatures Γ is small[29] and an efficient relaxation can occur. The less strained interface gives rise to smaller variations in local defect environment over the various sites leading to a lower $\sigma g_\perp$. On the microscopic level, at the high anneal temperature, the interface may rearrange interfacial bonds and bond angles to attain a lower energetic state.

Next, we may compare the difference in strain in the reference sample (Ia, Ib) for both crystallographic interface orientations as exposed by the $\sigma g_\perp$ values. Compared to data of P_b in (111)Si/SiO_2, it is observed that the (100)Si/SiO_2 interface, as jointly exposed by P_{b0} and P_{b1}, exhibits the highest strain (cf. Table I).

In a former study by Kobeda and Irene[26] the latter result was also inferred from measurements of interface strain (sample curvature) by using a double beam (He-Ne laser) reflection technique. The results were explained using a surface step model proposed by Mott[30] and later results of Leroy, which showed how SiO_2 may form on Si without the necessity for the buildup of large intrinsic stress.[31] If oxidation takes place predominantely at steps, the volume expansion advances laterally as well as normal to the surface. In

this manner a large fraction of the stress is relieved as the film grows. In comparing (111) and (100)Si orientations, Hahn and Henzler[22] reported a factor of 2 larger density of edge atoms at $(111)Si/SiO_2$ interfaces than in $(100)Si/SiO_2$ which would thus account for the lower strain at the $(111)Si/SiO_2$ interface. Yet, as later results showed that oxidation occurs not at edges but across terraces,[32] the latter model is not tenable. However, in another tentative view one may put that if the lateral volume expansion is limited by terrace bounding ledges, the lateral range for relaxation at the rougher $(100)Si/SiO_2$ interface will on the average be smaller, thus leading to an enhanced strained interface. In contrast, at the smooth $(111)Si/SiO_2$ interface the newly formed oxide is not confined in a specific area but can relax in all directions over the interface layer.

VI. CONCLUSIONS

A frequency-dependent ESR study of P_b-type interface defects has enabled us to quantify the interface strain at both (111) and $(100)Si/SiO_2$ interfaces. In contrast with the field-angle-dependent technique, which is complicated by anisotropic dipolar broadening and/or spectral overlap, this method is generally applicable.

In standard Si/SiO_2 ($T_{ox}\sim 970\,^{\circ}C$) the inferred values for $(100)Si/SiO_2$ of the strain induced variations in $g_\perp$ are $\sigma g_\perp \sim 0.0014$ and 0.0010 for P_{b0} and P_{b1}, respectively. These values are distinctly higher than the one obtained for P_b ($\sigma g_\perp \sim 0.000\,76$) in $(111)Si/SiO_2$, showing that $(100)Si/SiO_2$ exhibits generally more interface strain.

Post oxidation vacuum annealing at high temperatures ($\geqslant 1130\,^{\circ}C$) is found to affect both interfaces similarly, i.e., a drastic reduction of interface strain. This is mirrored in the drop of $\sigma g_\perp$ towards $\sim 0.000\,46$ and $\sim 0.000\,54$ for P_b and P_{b1}, respectively. These results expose the P_b-type defects, as reflected in their ESR properties, as most adequate probes of the interface strain.

The outlined fitting procedure allows, by extrapolation to $\nu \rightarrow 0$, to infer the residual linewidth, composed of only the intrinsic and the dipolar part. As to defect distributions in standard Si/SiO_2, the dipolar contributions indicate that P_{b0} and P_{b1} exhibit an enhanced 3D aspect in comparison with P_b, which reside preferably at 2D terraces.

However, at the (100) interface, peculiar increases in dipolar contributions are observed both for P_{b1} after high-temperature ($1130\,^{\circ}C$) POVA and for P_{b0} in low-T_{ox} samples, exposing that the interface roughness is dependent on sample treatment. The results can be qualitatively correlated with acquired insight from previous studies on interface roughness based on kinetic thermal smoothening and oxidation induced roughening: (i) The $(100)Si/SiO_2$ interface is rougher than typical for $(111)Si/SiO_2$; (ii) postoxidation thermal annealing in inert ambient drastically reduces roughness at $(100)Si/SiO_2$ interfaces; (iii) interface roughness is dependent on the oxidation rate.

[1] R. Helms and E. Pointdexter, Rep. Prog. Phys. **57**, 791 (1994).
[2] K. Brower, Appl. Phys. Lett. **43**, 1111 (1983).
[3] P. J. Caplan, E. H. Pointdexter, B. E. Deal, and R. R. Razouk, J. Appl. Phys. **50**, 5847 (1979).
[4] A. Stesmans, Appl. Phys. Lett. **48**, 972 (1986).
[5] A. Stesmans, Phys. Rev. B **48**, 2418 (1993).
[6] E. Pointdexter, P. Caplan, B. Deal, and R. Razouk, J. Appl. Phys. **52**, 879 (1981).
[7] A. Stesmans and V. V. Afanas'ev, J. Phys.: Condens. Matter **10**, L19 (1998).
[8] H. J. von Bardeleben, D. Stievenard, A. Grosman, C. Ortega, and J. Siejka, Phys. Rev. B **47**, 10 899 (1993).
[9] F. C. Rong, J. F. Harvey, E. H. Pointdexter, and G. J. Gerardi, Appl. Phys. Lett. **63**, 920 (1993).
[10] A. Stesmans and V. V. Afanas'ev, J. Appl. Phys. **83**, 2449 (1997).
[11] A. Stesmans and V. V. Afanas'ev, Appl. Phys. Lett. **72**, 2271 (1998).
[12] A. Stesmans, B. Nouwen, and V. V. Afanas'ev, Phys. Rev. B **58**, 15 801 (1998).
[13] K. L. Brower, Phys. Rev. B **33**, 4471 (1986).
[14] A. Stesmans and J. Braet, in *Insulating Films on Semiconductors*, edited by J. J. Simone and J. Buxo (North-Holland, Amsterdam, 1986), p. 25.
[15] G. D. Watkins and J. W. Corbett, Phys. Rev. **134**, 1359 (1964).
[16] G. Van Gorp and A. Stesmans, Phys. Rev. B **45**, 4344 (1992).
[17] A. Stesmans and B. Nouwen, Phys. Rev. B **61**, 16 068 (1999).
[18] K. L. Brower and T. J. Headley, Phys. Rev. B **34**, 3610 (1986).
[19] X. Chen and J. M. Gibson, Appl. Phys. Lett. **70**, 1462 (1997).
[20] X. Chen and J. M. Gibson, J. Electrochem. Soc. **146**, 3032 (1999).
[21] N. Awaji, S. Ohkubo, T. Nakanishi, K. Takasaki, and S. Komiya, Appl. Surf. Sci. **117–118**, 221 (1997).
[22] P. O. Hahn and M. Henzler, J. Vac. Sci. Technol. A **2**, 574 (1984).
[23] E. P. EerNisse, Appl. Phys. Lett. **30**, 290 (1977).
[24] E. A. Irene, E. Tierney, and J. Angillelo, J. Electrochem. Soc. **129**, 2594 (1982).
[25] E. Kobeda and E. A. Irene, J. Vac. Sci. Technol. B **4**, 720 (1986).
[26] E. Kobeda and E. A. Irene, J. Vac. Sci. Technol. B **5**, 15 (1987).
[27] Probably, a more correct term here woud be just ''structural relaxation''.
[28] Here, one may object that the $(100)Si/SiO_2$ reference sample Ib, grown at $T_{ox}=970\,^{\circ}C$, was subjected to PO treatments at $795\,^{\circ}C$. However, as this is significantly below T_{ox}, the interface will likely remain typical for that grown at $T_{ox}=970\,^{\circ}C$ (i.e., the highest process temperature underwent).
[29] J. T. Fitch, E. Kobeda, G. Lucovsky, and E. A. Irene, J. Vac. Sci. Technol. B **7**, 153 (1989).
[30] N. F. Mott, Philos. Mag. A **45**, 323 (1981).
[31] B. Leroy, Philos. Mag. B **55**, 159 (1987).
[32] F. M. Ross and J. M. Gibson, Phys. Rev. Lett. **68**, 1782 (1992).